Modeling and Control of Flexible HEV Charging Station upgraded with Flywheel Energy Storage

Dragicevic, Tomislav; Shafiee, Qobad; Wu, Dan; Meng, Lexuan; Vasquez, Juan Carlos; Guerrero, Josep M.

Published in:
Proceedings of the 11th International Multi-Conference on Systems, Signals and Devices, SSD 2014

DOI (link to publication from Publisher):
10.1109/SSD.2014.6808864

Publication date:
2014

Document Version
Early version, also known as pre-print

Modeling and Control of Flexible HEV Charging Station upgraded with Flywheel Energy Storage

Tomislav Dragičević, Qobad Shafiee, Dan Wu, Lexuan Meng, Juan C. Vasquez, and Josep M. Guerrero

***Abstract*—This paper deals with the design of a fast DC charging station (FCS) for hybrid electric vehicles (HEVs) that is connected at a remote location. Power rating of this new technology can go up to a hundred kW and it represents a main challenge for its broad acceptance in distribution systems. In that sense, growing number of these stations, if operated in a non-flexible regime, will start to cause problems in future distribution systems such as overloads of local network's corridors and reduction of its total equivalent spinning reserves. A power balancing strategy based on a local energy storage system (ESS) is proposed in this paper. Flywheel has been selected as the means of storing energy as it provides high power density and does not have significant performance degradation along its lifetime. Implemented control algorithm uses the energy stored in flywheel to compensate for the peak of power introduced by HEV charger, avoiding big initial stress in grid converter and also is able to limit the maximum extracted power. In addition, feed-forward compensation has been implemented to reduce the voltage dip within the station. Real time simulation results, that prove the validity of proposed approach, have been presented.**

***Index Terms*—Fast charging station (FCS), hybrid electric vehicle (HEV), flywheel.**

I. Introduction

GREATER electrification of the transport sector by introducing the concept of hybrid electric vehicle (HEV) opens up many possibilities for supporting the shift towards cleaner electricity. Moreover, HEV architecture strongly underpins the current trends in automotive industry where more and more attention is devoted to the increase of the customer comfort level in terms of installing various additional electrical appliances [1]. By replacing whole or part of the propulsion system in conventional vehicles with electrical engines and using the grid power for recharging the MEV's battery pack, an on-going utility shift towards more renewable systems may be conveyed to the transportation sector as well.

Plug in HEVs are expected to play a significant role in the overall workload of future distribution networks and hence creation of safe environment for their smooth acceptance is one of critical smart grid (SG) objectives [2]. Combined impact of a large number of randomly connected HEV chargers on the distribution network is the main concern [3], [4]. Fast charging stations (FCS) with power rating of up to 100 kW have a particularly adverse impact in that sense [5] as their combined effect may even have a reflection on the spinning reserve of the power system [6] or cause equipment overload [7], [8].

The aim of this paper is to address the problem by introducing a dedicated energy storage system (ESS) connected to the DC side of the station in order to counterbalance the high power requirement of HEV charger. There have been approaches in the past that try to elaborate on a similar idea of forming a power buffer around the common DC link [9]–[11], but in none of those a full recharging pattern for a battery was considered and only static technologies were assessed.

On the contrary, a low speed flywheel has been used in this paper, extending the concept commonly used for balancing of production variations of wind parks [12]–[14]. The novelty introduced here involves essentially decentralized control principle, the correct operation of which relies on detection of the voltage variations in the common DC bus. This type of control strategy is commonly referred to as distributed bus signaling (DBS) strategy and was in the past extensively applied for control of DC microgrids [15]–[17]. To that end, several strategies that alleviate the impact of charging station on utility mains are discussed, analyzed and simulated in this paper. On top of DBS management backbone, two additional enhancements have been implemented; 1) feed-forward compensation of HEV charging current and 2) reactive power controller that enhances local voltage conditions.

The paper is organized as follows. Section II reveals the configuration of FCS. In Section III, a DBS method is proposed to achieve decentralized coordination between all units and the full scale control architecture used for simulation platform is presented. Real-time power hardware in the loop simulation results are presented in Section IV. Finally, Section V gives the conclusion.

II. Configuration of a DC Fast Charge Station

Fig. 1 shows a schematic diagram of FCS supplemented with the flywheel ESS. Associated power stage consists of a HEV charger and a pair of two-level inverters, where one serves as a grid interface while the other enables a variable speed operation of the flywheel and hence the restorability of energy. 650 V was chosen as the nominal value of the common DC bus, since it is higher than fully charged voltage of any commercially available HEV battery and it thus permits applicability of buck DC/DC converters as chargers [18].

The overall control of CS is divided into two layers organized into a hierarchical structure, following the common principle for management of both large interconnected and small distributed generation (DG) systems [19], [20]. Respective layers are separated by bandwidths, with the latter being the closest to the physical equipment termed as primary layer and the one on top of it as secondary layer. The speed of primary layer is bounded by the switching frequencies of grid-tied and ESS converters and its response time is generally set to about one tenth of that value [21]. Bandwidth of secondary layer is normally reduced for an additional order of magnitude.

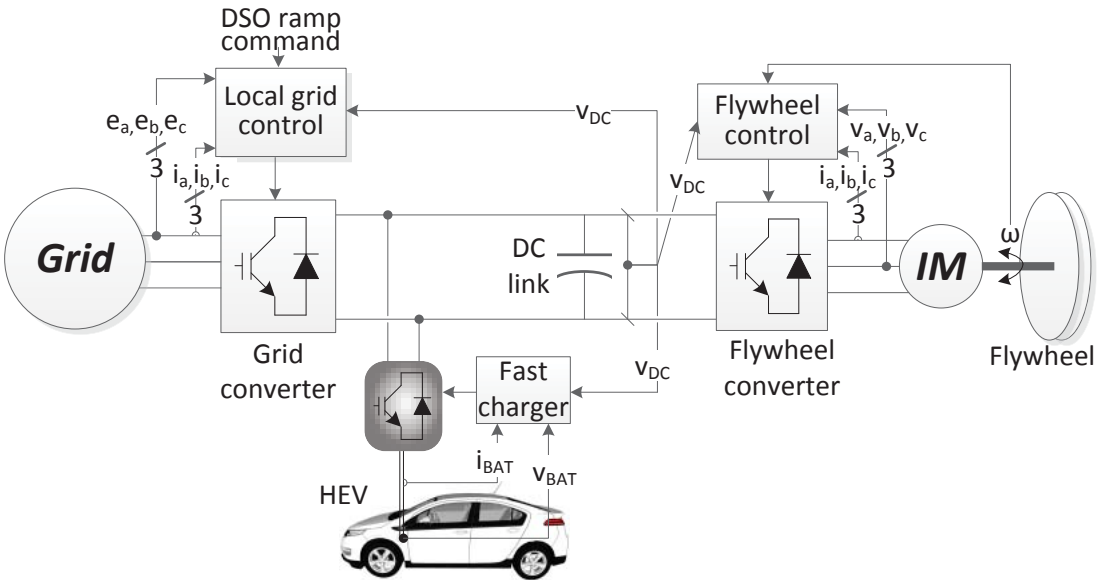

Fig. 1. Diagram of a pHEV fast charging station.

In this way, it is possible to design both layers independently from each other [22].

Design of the primary layer was carried out considering the features of physical equipment, particularly the switching frequencies of grid and ESS converters and their respective filters [23]. For that matter, an averaged models of converters were considered for tuning of control parameters and for the simulation of whole system. On the other hand, secondary layer is concerned with handling the power exchange with the network, and with that aim, several control strategies have been implemented primarily focusing on the response of the grid converter in the event of HEV connection. More particularly, the functionalities such as the ramp increase of power, limitation of the total consumption and provision of voltage support services have been developed.

By inspecting the system diagram shown in Fig. 1, one may derive the dynamic representation of the system according to current balance in DC-link capacitor

$$C_{DC}\frac{dv_{DC}}{dt} = i_{grid} + i_{fly} - i_{HEV} \tag{1}$$

where C_{DC} is the common DC bus capacitance, i_{grid} and i_{fly} are DC currents going from the grid and flywheel toward the bus, whereas i_{HEV} is the current extracted by the fast DC charger. Since each of these components has its own dynamic properties, their impact needs to be studied analytically so as to check the stability properties and calculate the appropriate gains of feed-forward compensation. First step in that sense is to analyze the primary control layer. So, three components that appear in this system are as follows.

A. HEV charger

HEV charger is a buck DC/DC converter with pre-installed HEV battery charging algorithm which comprises constant current and constant voltage stages. Since current and voltage in question are related only with battery, this system does not need any feedback signals from FCS. In addition, the regulation speed of this process is not of critical importance, and a low bandwidth controller is normally derived. All that being said, it can be concluded that the current introduced by the HEV charger may be considered as a disturbance input that does not have an impact on dynamic properties of the system.

B. Grid interface

Grid interface is a two level rectifier modeled in d-q reference frame which rotates in synchronism with the grid voltage, assured by the phase locked loop (PLL). Model of rectifier in d-q rotating reference frame can be expressed as [24]:

$$\begin{bmatrix}\dot{i_d}\\ \dot{i_q}\end{bmatrix} = \frac{v_{DC}}{L}\begin{bmatrix}d_d\\ d_q\end{bmatrix} + \begin{bmatrix}-\frac{R}{L} & \omega\\ -\omega & -\frac{R}{L}\end{bmatrix}\begin{bmatrix}i_d\\ i_q\end{bmatrix} - \frac{1}{L}\begin{bmatrix}e_d\\ e_q\end{bmatrix} \tag{2}$$

where i_q and i_d, d_q and d_d are DC-like currents and duty ratios aligned with q and d rotating axes, respectively, while R_{line} and L are per phase resistance and inductance of the AC line.

It can be easily shown that with a feed-forward compensation that nullifies the cross-coupling terms, and tuning of control parameters (with aim of canceling the pole in the $R-L$ element of the line), the converter will follow reference currents imposed upon it with only a first order delay [24]. Following nonlinear expression shows a DC current flowing towards the common bus

$$i_{grid} = 1.5\frac{v_d i_d}{v_{DC}}. \tag{3}$$

Notice that there is no q terms in the expression. This is due to a fact that PLL synchronizes the grid voltage with d-axis, fixing the q-axis voltage always to zero. (3) may be linearized around the operating DC voltage, obtaining

$$\hat{i_{grid}} = 1.5\frac{(\,e_d + 2\,I_d\,R + I_d\,L\,s)}{V_{DC}}\hat{i_d} \tag{4}$$

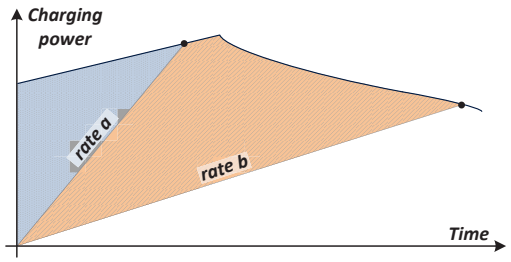

Fig. 2. Analysis of charging profile when subjected to rate limit control strategy.

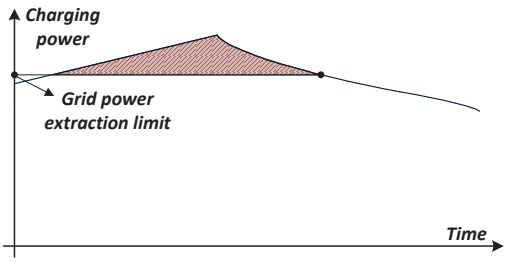

Fig. 3. Analysis of charging profile when subjected to limited grid power extraction control strategy.

Where I_d is the equilibrium value of i_d. The reference for i_d is generated by the upper control layer, the principle of which is presented in the next Section.

C. Flywheel

Flywheel ESS is a bidirectional inverter connected to a squirrel cage IM. The dynamics of this subsystem are governed by the machine parameters and the settings of associated control loops. Standard vector control has been considered as an internal scheme because it provides rapid and accurate torque response [25]. Again, a rotating reference frame is used for modeling and control of the machine. However, unlike the grid voltage, flux of the machine is followed in this case. Based on this assumption, the d-q model in flux coordinates can be represented as follows

$$\begin{bmatrix}\dot{i_d}\\ \dot{i_q}\end{bmatrix} = \frac{v_{DC}}{\sigma L_s}\begin{bmatrix}d_d\\ d_q\end{bmatrix} + \begin{bmatrix}-\frac{R_s}{\sigma L_s} & \omega_{mR}\\ -\omega_{mR} & -\frac{R_s}{\sigma L_s}\end{bmatrix}\begin{bmatrix}i_d\\ i_q\end{bmatrix} - \frac{1}{\sigma L_s}\begin{bmatrix}0\\ \omega_{mR}\psi_r\frac{L_0}{L_r}\end{bmatrix} \tag{5}$$

where L_0 is the machine's mutual inductance, whereas L_s, L_r, R_s, R_r are stator and rotor inductances and resistances, respectively; i_d and i_q d and q-axis currents in field coordinates, ω_{mR} is the flux rotational speed, i_{mR} is the magnetizing current, while ψ_r is the rotor flux; σ is the total leakage coefficient, defined as

$$\sigma = 1 - \frac{1}{(1+\sigma_S)(1+\sigma_R)}, \tag{6}$$

where

$$\sigma_s = 1 - \frac{L_s}{L_0}, \sigma_r = 1 - \frac{L_r}{L_0}. \tag{7}$$

The magnetizing current i_{mR} and i_d are related with

$$L_r\frac{di_{mR}}{dt} = R_r(i_d - i_{mR}), \tag{8}$$

while the link between field and rotor orientation is given by

$$\omega_{mR} = \omega_{rot} + \frac{R_r i_q}{L_r i_{mR}} \tag{9}$$

where ω_{rot} is the rotational speed of the rotor.

The inner current loops are tuned following the same principle as in the case of grid converter. Then, i_d and i_q follow their references just as a first order delay and DC current of a flywheel is

$$i_{fly} = 1.5\frac{v_d i_d + v_q i_q}{v_{DC}}. \tag{10}$$

Now, if (5) is put into (10), with a bit of algebraic manipulations of (6) to (9), linearized expression around V_{DC} may be derived as

$$\hat{i_{fly}} = 1.5\frac{2\left(R_s + \left(\frac{L_0}{Lr}\right)^2 R_r\right) I_q + \frac{\omega_{rot0}L_0^2 I_d}{L_r} + \sigma L_s I_q s}{V_{DC}}\hat{i_q}, \tag{11}$$

where I_q, I_d are the equilibrium values for currents in field coordinates, whereas ω_{rot0} is the instantaneous rotational speed.

Swing equation of the flywheel governs the changes in the rotational speed of the rotor

$$J\frac{d\omega_{rot}}{dt} = T_{el} = 1.5p(1-\sigma)L_s i_{mR} i_q, \tag{12}$$

where J is the flywheel inertia, and p is the number of pole pairs.

III. Control of FCS

The aim of the supervisory control is to balance the current injection/extraction from grid, flywheel and HEV. To that end, energy stored in flywheel is used to counterweight the impact of a sudden start of HEV charging by making the grid converter following some predetermined pattern of conduct. In that sense, it can be programmed to

1) Increase the current according to maximum permitted rate until it equalizes with the HEV current.
2) Limit the maximum power extraction from the grid

Without losing any generality, both strategies can be implemented at the same time. Depending on permitted rate limit and total power limit, required available storage energy can be calculated. This is elaborated in the following subsection.

A. Calculation of Required Flywheel Inertia

A typical power profile in case of fast charging for the HEV is depicted in Fig. 2 [26]. It is divided into two principal stages; first one is characterized by a constant current and rising voltage, whereas the second one by constant voltage and decreasing current.

Following the first strategy suggested in previous subsection, one may see that depending on allowed rate of GC current increase, the intersection between upper boundary and fixed rate will occur in the first or second stage. Therefore, the flywheel energy demand for this application can be defined

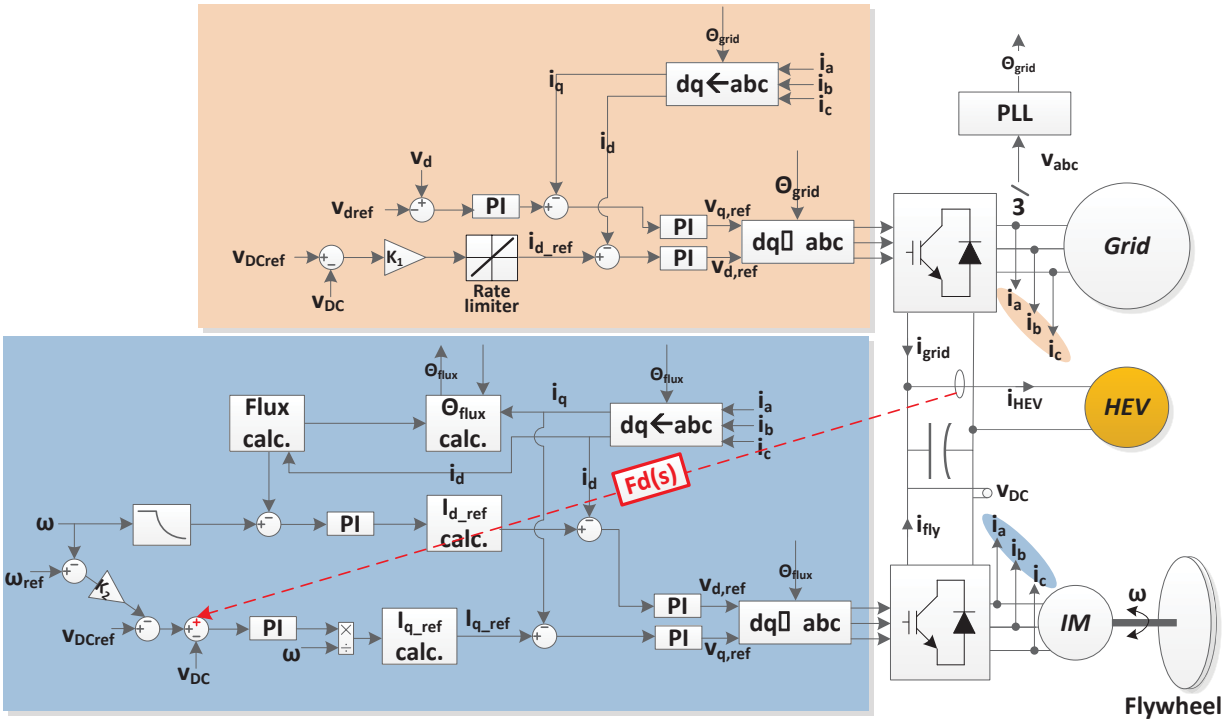

Fig. 4. Flywheel and grid converter control schemes with feedforward compensation and grid voltage support.

as an area surrounded by the upper boundary and the line that indicates the maximum slope of GC. Fig. 2 also shows how this area gets larger with the decreasing permissible slope. Knowing the typical charging profile for the given HEV, the respective area may be derived as

$$E_{fly} = \int_0^{\Delta T} P_{ch} dt - rate \cdot \Delta T. \tag{13}$$

where ΔT is the period from beginning of charging until the intersection of GC and HEV powers. P_{ch} is the instantaneous power extracted by HEV charger. Since the energy stored in flywheel is given by

$$E_{fly} = J\frac{\omega_{rot}^2}{2}, \tag{14}$$

the minimum required inertia may be derived taking into account the nominal rotational speed

$$J_1 = 2\frac{\int_0^{\Delta T} P_{ch} dt - rate \cdot \Delta T}{\omega_{rot}^2}. \tag{15}$$

On the other hand, if the limited power extraction from the grid strategy is considered, the calculation of required ESS energy and hence also the inertia of the flywheel is a bit different. It can be analyzed by observing Fig. 3. In this case (15) is transformed into

$$J_2 = 2\frac{\int_0^{\Delta T} P_{ch} dt - P_{gmax}}{\omega_{rot}^2}. \tag{16}$$

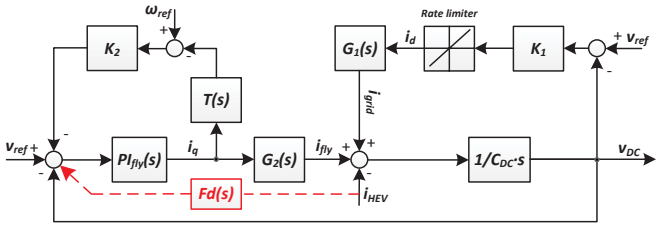

Fig. 5. Reduced order block diagram.

where P_{gmax} is the maximum permitted power extraction from the grid.

If both strategies are considered at the same time, than actual J should be selected as the maximum of J_1 and J_2. It should be noticed than imposing current reference in this case is virtually proportional to the output power since the common DC voltage is regulated within the tight boundaries and v_d voltage at point of common coupling (PCC) is also tightly regulated, as it will be discussed in the following subsection.

B. Proposed Control Strategy

Decentralized supervisory control was implemented in this paper. It generates references for inner current loops of active converters for grid and flywheel interface. Since both converters are programmed to regulate the common voltage, some sort of non-stiff control was needed to be designed. For that purpose, a voltage vs. rotational speed droop control law was put into the flywheel so that the grid converter always has an information about the state of charge (SOC).

Controller of GC was designed as a sole proportional gain in d-axis after which it was possible to implement different

functionalities as elaborated in preceding discussions. Then, according to voltage deviation in the common bus, the controller determines the i_d portion of the current to be injected. On the other hand, the controller in q-axis is a classical PI controller tuned to a speed that is around an order of magnitude slower than the inner current loop. It determines the injection of reactive power in order to restore the voltage in the PCC back to nominal value.

A full hierarchical control structure of the system is shown in Fig. 4. The respective structure may be directly translated to a reduced order model which is needed to calculate the transfer function used for the feed-forward compensation.

C. Feedforward Compensation

Reduced order diagram was constructed using the reasonable simplification in which the inner current loops together with corresponding $R-L$ elements are considered to instantaneously follow imposed references. Then, DC currents are approximated by small signal expressions (4) and (11).

Resulting diagram is shown in Fig. 5. By its inspection one may notice the input point of HEV current. G_1 and G_2 represent transfer functions from i_d and i_q to i_{grid} and i_{fly}. K_1 and K_2 indicate the proportional term of the voltage controller in GC and droop coefficient in FC, respectively. F represents the machine's swing equation. PI_{fly} is the FC voltage controller, defined as $k_{pq}+k_{iq}/s$.

As already discussed, since the charging process of HEV is regulated by a low bandwidth controller, it can be considered as a disturbance input to the system. Therefore, the transfer function $Fd(s)$ that theoretically completely cancels the dip in the common DC bus voltage following step change in HEV current can be analytically calculated. The path of feed-forward compensation is indicated with dotted red line, while the derivation of correct transfer function is given below. It is noticed here that flywheel is selected as a unit which performs the disturbance compensation since the grid converter is rate limited.

The principle of canceling the impact of one of the disturbances to the system is first to calculate the transfer function from the respective disturbance to the output, G_{dis}, and a transfer function from the input of the main compensator of the system to output $G_{sys}(s)$, respectively. Then, given that it is possible to measure the examined disturbance, it should be feed-forwarded to the input of compensator using a gain $Fd(s)$ that enforces the following relationship $G_{dis(s)}$-$G_{sys(s)} \times Fd(s) = 0$. Now, returning back to Fig. 5, one may easily calculate that $Fd(s)$ which meets that requirement is

$$Fd(s) = \frac{1}{G_2 \cdot PI_{fly}} \tag{17}$$

where G_2 obtained from (11). It should be noted that the droop control law has been intentionally neglected in derivation of the feed-forward transfer function (17) as the voltage deviation would also be compensated for with its inclusion, which would compromise the performance of the system. The feed-forward control law has been encompassed within the full model of the plant and its response details are presented in the following section.

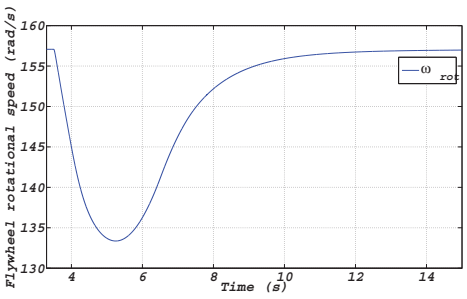

Fig. 6. Flywheel speed propagation throughout the rate limit power strategy transient.

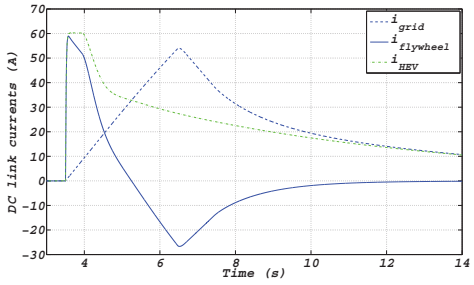

Fig. 7. DC current propagation throughout the rate limit power strategy transient.

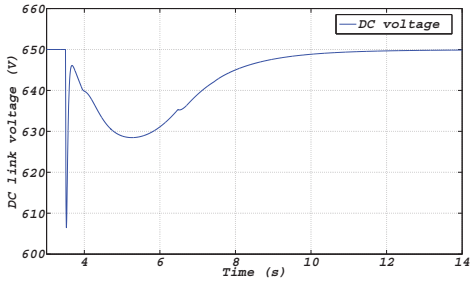

Fig. 8. Common DC voltage propagation throughout the rate limit power strategy transient.

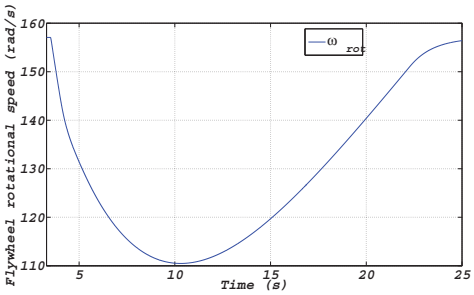

Fig. 9. Flywheel speed propagation throughout the constant power strategy transient.

IV. Simulation Results

Complete model of the system shown in Fig. 4 was constructed in Matlab/Simulink and compiled into dSPACE 1006. The parameters needed for performing the simulation are given in Table I. For the matter of speeding up the simulation time,

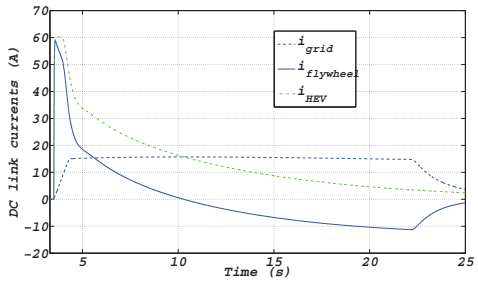

Fig. 10. DC current propagation throughout the constant power strategy transient.

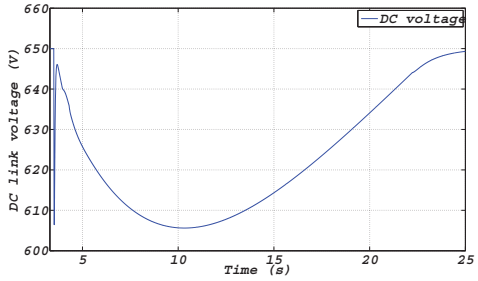

Fig. 11. Common DC voltage propagation throughout the constant power strategy transient.

the capacity of the HEV's battery was down-scaled to $0.2Ah$ and rate limit for i_d current of GC was set to $25A/s$. Battery model used for emulating HEV was the same as in [17], but with appropriately scaled voltage. The length of line was selected to be 5 km, and flywheel inertia was selected to be $10kgm^2$, as it was enough to comply with down-scaled battery model.

Two basic simulation studies have been performed which include: Rate strategy and power limit strategy which encompasses both rate limit and power limit.

For the first case, with allowable i_d rate being set to $25A/s$ Fig. 6 shows the full propagation of flywheel rotational speed from the starting moment of HEV charging ($t = 3.5s$), until the its full recharge. In Fig. 7 and Fig. 8, propagation of DC currents and common DC voltage can be seen, respectively. It can be seen that the initial HEV current is compensated by the FC, while GC operates in rate saturated mode and slowly increases its current. Some time after the sum of HEV and

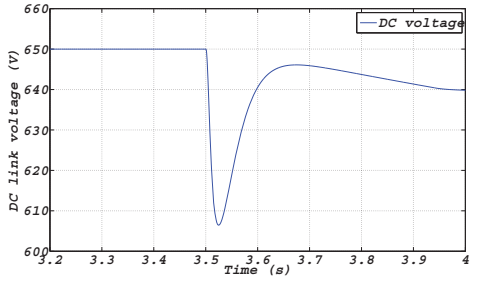

Fig. 12. Common DC voltage before feed-forward compensation.

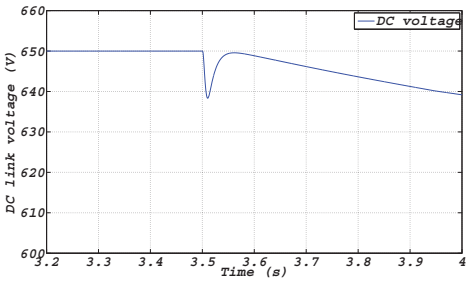

Fig. 13. Common DC voltage after feed-forward compensation.

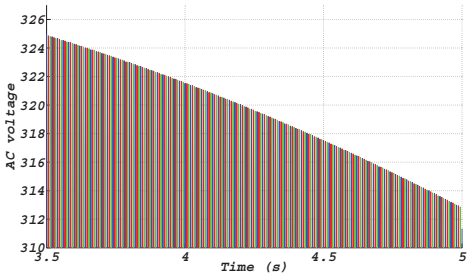

Fig. 14. Voltages at PCC before reactive power compensation.

FC current equalize with those of GC, it exits the saturated mode and starts regulating the common DC voltage, eventually reaching the steady state value of 650 V (while at the same time recharging the flywheel).

Second case which comprises both rate and total current limit (set to 20 A), the same HEV charging pattern is being depicted in Figs. 6, 7 and Fig. 8. It can be observed that more energy is extracted from the flywheel due to limited current extraction from the grid.

Feed-forward and reactive power compensation basically operate independently on the imposed supervisory strategy due to rate limiter which is active in both applications. Figs. 12 and 13 show the zoomed in capture of a transient before and after a feed forward compensation has been applied. Significant improvement can be seen, but still the dip is not completely canceled. This is mainly due to delays of inner current loops. Figs. 14 and 15 show the zoomed in capture of PCC voltages before and after application of reactive power compensator. Again, good improvement of the PCC voltages can be observed.

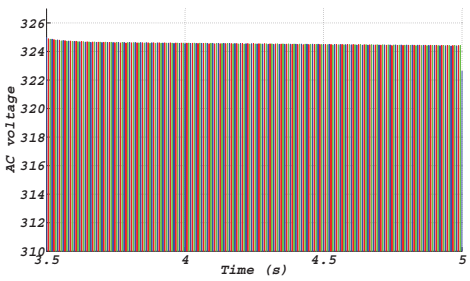

Fig. 15. Voltages at PCC after reactive power compensation.

TABLE I
REAL-TIME SIMULATION SETUP PARAMETERS

Parameter	Value
Electrical parameters	
C_{DC}	$2.2mF$
L_{filt}	$3.8mH$
R_{filt}	0.24Ω
$V_{grid,nom}(p-p)$	$325V$
HEV	
T_{HEV}	$0.02s$
$Capacity$	$0.2Ah$
Induction machine	
L_0	$10.46mH$
L_s	$10.76mH$
L_r	$10.76mH$
R_s	0.0148Ω
R_r	0.0093Ω
σ	0.055
J	$10\ kgm^2$
Flywheel control	
T_{fly}	$0.00025s$
kp_q	3
ki_q	100
ω_{ref}	$1500rpm$
K_2	0.1
Grid rectifier control	
T_{grid}	$0.00025s$
K_1	2.575
i_{drate}	$25A/s$
Distribution line parameters	
L	$0.2mH/km$
R	$0.268\Omega/km$

V. CONCLUSION

This paper proposes two control strategies for counterbalancing the adverse impact of HEV FCS on electric utility. The principle of operation is exploitation of dedicated ESS which provides either the peak of power or continuous supply until the time the grid current on DC equalizes with HEV current. Apart from principal control that is based on DBS and ensures decentralized coordination between units, a feed-forward compensation has been analytically derived. Also, the voltage drop effects which are expected in the case when FCS is connected to a weak grid, have been compensated for using the reactive power regulator. The validity of proposed system oriented approach has been verified by real time simulation results.

REFERENCES

[1] A. Emadi, M. Ehsani, and J. Miller, *Vehicular Electric Power Systems: Land, Sea, Air, and Space Vehicles*. The Power engineering, Taylor & Francis, 2010.

[2] "European Technology Platform SmartGrids: Strategic Research Agenda: Update of the SmartGrids SRA 2007 for the needs by the year 2035." http://www.smartgrids.eu/documents/sra2035.pdf, 2012. [Online; accessed 13-October-2013].

[3] Z. Fan, "A distributed demand response algorithm and its application to phev charging in smart grids," *Smart Grid, IEEE Transactions on*, vol. 3, no. 3, pp. 1280–1290, 2012.

[4] D. Steen, L. Tuan, O. Carlson, and L. Bertling, "Assessment of electric vehicle charging scenarios based on demographical data," *Smart Grid, IEEE Transactions on*, vol. 3, no. 3, pp. 1457–1468, 2012.

[5] M. Yilmaz and P. Krein, "Review of battery charger topologies, charging power levels, and infrastructure for plug-in electric and hybrid vehicles," *Power Electronics, IEEE Transactions on*, vol. 28, no. 5, pp. 2151–2169, 2013.

[6] P. Kundur and N. J. Balu, *Power System Stability and Control*. McGraw-Hill, 1998.

[7] K. Clement-Nyns, E. Haesen, and J. Driesen, "The impact of charging plug-in hybrid electric vehicles on a residential distribution grid," *Power Systems, IEEE Transactions on*, vol. 25, no. 1, pp. 371–380, 2010.

[8] K. Qian, C. Zhou, M. Allan, and Y. Yuan, "Modeling of load demand due to ev battery charging in distribution systems," *Power Systems, IEEE Transactions on*, vol. 26, no. 2, pp. 802–810, 2011.

[9] A. Hajizadeh, M. Golkar, and A. Feliachi, "Voltage control and active power management of hybrid fuel-cell/energy-storage power conversion system under unbalanced voltage sag conditions," *Energy Conversion, IEEE Transactions on*, vol. 25, no. 4, pp. 1195–1208, 2010.

[10] H. Hoimoja, A. Rufer, G. Dziechciaruk, and A. Vezzini, "An ultrafast ev charging station demonstrator," in *Power Electronics, Electrical Drives, Automation and Motion (SPEEDAM), 2012 International Symposium on*, pp. 1390–1395, 2012.

[11] O. Laldin, M. Moshirvaziri, and O. Trescases, "Predictive algorithm for optimizing power flow in hybrid ultracapacitor/battery storage systems for light electric vehicles," *Power Electronics, IEEE Transactions on*, vol. 28, no. 8, pp. 3882–3895, 2013.

[12] R. Cardenas, R. Pena, G. Asher, J. Clare, and R. Blasco-Gimenez, "Control strategies for power smoothing using a flywheel driven by a sensorless vector-controlled induction machine operating in a wide speed range," *Industrial Electronics, IEEE Transactions on*, vol. 51, no. 3, pp. 603–614, 2004.

[13] S. Samineni, B. Johnson, H. Hess, and J. Law, "Modeling and analysis of a flywheel energy storage system for voltage sag correction," *Industry Applications, IEEE Transactions on*, vol. 42, no. 1, pp. 42–52, 2006.

[14] G. Cimuca, C. Saudemont, B. Robyns, and M. Radulescu, "Control and performance evaluation of a flywheel energy-storage system associated to a variable-speed wind generator," *Industrial Electronics, IEEE Transactions on*, vol. 53, no. 4, pp. 1074–1085, 2006.

[15] J. Schonberger, R. Duke, and S. Round, "DC-Bus Signaling: A Distributed Control Strategy for a Hybrid Renewable Nanogrid," *IEEE Transactions on Industrial Electronics*, vol. 53, pp. 1453–1460, Oct. 2006.

[16] K. Sun, L. Zhang, Y. Xing, and J. M. Guerrero, "A Distributed Control Strategy Based on DC Bus Signaling for Modular Photovoltaic Generation Systems With Battery Energy Storage," *IEEE Transactions on Power Electronics*, vol. 26, pp. 3032–3045, Oct. 2011.

[17] T. Dragicevic, J. Guerrero, J. Vasquez, and D. Skrlec, "Supervisory control of an adaptive-droop regulated dc microgrid with battery management capability," *Power Electronics, IEEE Transactions on*, vol. 29, no. 2, pp. 695–706, 2014.

[18] M. Ehsani, Y. Gao, and A. Emadi, *Modern Electric, Hybrid Electric, and Fuel Cell Vehicles: Fundamentals, Theory, and Design, Second Edition*. Power Electronics and Applications Series, Taylor & Francis, 2009.

[19] J. Machowski, J. W. Bialek, and J. R. Bumby, *Power System Dynamics: Stability and Control*. John Wiley-Sons, Ltd, 2008.

[20] F. Blaabjerg, Z. Chen, and S. Kjaer, "Power Electronics as Efficient Interface in Dispersed Power Generation Systems," *IEEE Transactions on Power Electronics*, vol. 19, pp. 1184–1194, Sept. 2004.

[21] M. Liserre, F. Blaabjerg, and S. Hansen, "Design and control of an lcl-filter-based three-phase active rectifier," *Industry Applications, IEEE Transactions on*, vol. 41, no. 5, pp. 1281–1291, 2005.

[22] J. M. Guerrero, J. C. Vasquez, J. Matas, L. G. de Vicuna, and M. Castilla, "Hierarchical Control of Droop-Controlled AC and DC MicrogridsA General Approach Toward Standardization," *IEEE Transactions on Industrial Electronics*, vol. 58, pp. 158–172, Jan. 2011.

[23] A. Yazdani and R. Iravani, *Voltage-Sourced Converters in Power Systems*. Wiley, 2010.

[24] V. Blasko and V. Kaura, "A new mathematical model and control of a three-phase ac-dc voltage source converter," *Power Electronics, IEEE Transactions on*, vol. 12, no. 1, pp. 116–123, 1997.

[25] W. Leonhard, *Control of Electrical Drives, Third edition*. Power Systems, Springer, 2001.

[26] S. Bai and S. Lukic, "Unified active filter and energy storage system for an mw electric vehicle charging station," *Power Electronics, IEEE Transactions on*, vol. 28, no. 12, pp. 5793–5803, 2013.